

Topological Structure of the QCD Vacuum Revealed by Overlap Fermions

Ernst-Michael Ilgenfritz, Karl Koller, Yoshiaki Koma, Gerrit Schierholz, and
Volker Weinberg

Abstract Overlap fermions preserve a remnant of chiral symmetry on the lattice. They are a powerful tool to investigate the topological structure of the vacuum of Yang-Mills theory and full QCD. Recent results concerning the localization of topological charge and the localization and local chirality of the overlap eigenmodes are reported. The charge distribution is radically different, if a spectral cut-off for the Dirac eigenmodes is applied. The density $q(x)$ is changing from the scale- a charge density (with full lattice resolution) to the ultraviolet filtered charge density. The scale- a density, computed on the Linux cluster of LRZ, has a singular, sign-coherent global structure of co-dimension 1 first described by the Kentucky group. We stress, however, the cluster properties of the UV filtered topological density resembling the instanton picture. The spectral cut-off can be mapped to a bosonic smearing procedure. The UV filtered field strength reveals a high degree of (anti)selfduality at “hot spots” of the action. The fermionic eigenmodes show a high degree of local chirality. The lowest modes are seen to be localized in low-dimensional space-time regions.

Ernst-Michael Ilgenfritz
Institut für Physik, Humboldt-Universität zu Berlin, 12489 Berlin, Germany
e-mail: ilgenfri@physik.hu-berlin.de

Karl Koller
Fakultät für Physik, Ludwig-Maximilians-Universität München, 80333 München, Germany
e-mail: Karl.Koller@lrz.uni-muenchen.de

Yoshiaki Koma
Numazu College of Technology, 3600 Ooka, Numazu-shi, Shizuoka 410-8501, Japan
e-mail: koma@numazu-ct.ac.jp

Gerrit Schierholz
Institut für Theoretische Physik, Universität Regensburg, 93040 Regensburg, Germany
Deutsches Elektronen-Synchrotron DESY, 22603 Hamburg, Germany
e-mail: gsch@mail.desy.de

Volker Weinberg
Leibniz-Rechenzentrum der Bayerischen Akademie der Wissenschaften,
85748 Garching b. München, Germany
e-mail: Volker.Weinberg@lrz.de

1 Introduction: Overlap Fermions and Topological Charge

Quantum chromodynamics (QCD) is the theory of strong interactions. It is formulated in terms of quarks and gluons. The task is twofold: to describe the composite structure and the high-energy interactions of strongly interacting *hadrons*, in both cases taking the substructure in terms of quarks and gluons into account. One problem for theorists and experimentalists is that quarks are permanently *confined* inside hadrons. Apart from details, the spectrum and symmetries of hadrons are dictated by an approximate *chiral symmetry* and its spontaneous breaking by the interaction via gluons. These properties are unique for QCD as part of the standard model and result from the vacuum fluctuations of gluons. At a temperature of about 160 MeV the hadronic world experiences a transition to a quark-gluon plasma phase with rather unusual properties. Then, the vacuum structure has changed.

Simulations on a space-time lattice are the only *ab initio* approach to these phenomena. This approach has the virtue that also structural information on the vacuum fluctuations is accessible. On the other hand, there are models attempting to give a qualitative understanding. Some of them, like the instanton model, were partially successful. The instanton model became challenged more recently. A study of how the *topological charge density* is distributed in space-time and how the gluon field localizes the quarks (in analogy to the Anderson effect) is crucial to understand the microscopic mechanisms.

Overlap fermions [1, 2] possess an exact chiral symmetry on the lattice [3] and realize the Atiyah-Singer index theorem at a finite lattice spacing a [4]. This is possible because they allow a clear distinction between chiral zero modes and non-chiral non-zero modes. Depending on their chirality, counting of n_+ or n_- zero modes determines the topological charge of the gauge field as $Q = n_- - n_+$. Furthermore, they give rise to a *local* definition of the topological charge density [5]. Altogether, this makes overlap fermions an attractive tool for investigating the chiral and topological structure of the QCD vacuum.

The topological structure attracts attention because of the old hope that local excitations contributing to the winding number might not only realize the breaking of $U_A(1)$ symmetry but simultaneously provide a mechanism for confinement and chiral symmetry breaking. The instanton liquid model (ILM) does not fulfill this expectation: it can account for chiral symmetry breaking but fails to give an explanation of confinement.

When the QCDSF collaboration had started to analyze ensembles of lattice configurations with overlap fermions for quenched QCD [6, 7] and later for QCD with dynamical quarks [8] by diagonalizing the massless overlap Dirac operator and to store an – until then unprecedented – number of eigenmodes ($\mathcal{O}(150)$ per configuration), the way was open for a serious investigation of the structure of topological charge [9–11]. Not long before we started this investigation, the instanton model had been challenged [12–14] by the observation that the topological charge, rather than appearing in $4d$ clusters, possesses a global, sign-coherent $3d$ membrane-like structure [15–17]. We shall discuss here what remains from the instanton picture.

The overlap Dirac operator D has to fulfill the Ginsparg-Wilson [18] equation,

$$\gamma_5 D^{-1} + D^{-1} \gamma_5 = a 2R \gamma_5, \quad (1)$$

with a local operator R . This is what maximally can remain of chiral symmetry on the lattice. A possible solution – for any input Dirac operator, i.e. for the Wilson-Dirac operator D_W as well – is the following zero mass overlap Dirac operator

$$D(m=0) = \frac{\rho}{a} \left(1 + \frac{D_W}{\sqrt{D_W^\dagger D_W}} \right) = \frac{\rho}{a} (1 + \text{sgn}(D_W)), \quad (2)$$

with $D_W = M - \frac{\rho}{a}$ where M is the Wilson hopping term and $\frac{\rho}{a}$ a negative mass term to be optimized. This operator is diagonalized using a variant of the Arnoldi algorithm. The operator can be improved by projecting the Ginsparg-Wilson circle on the imaginary axis, $\lambda \rightarrow \lambda_{\text{imp}}$. The topological density can be defined (with maximal resolution a) as follows:

$$q(x) = -\text{tr} \left[\gamma_5 \left(1 - \frac{a}{2} D(m=0; x, x) \right) \right]. \quad (3)$$

Using the spectral representation of (3) in terms of the eigenmodes $\psi_\lambda(x)$ with eigenvalue λ , an UV smoothed form of the density can be defined by filtering,

$$q_{\lambda_{\text{sm}}}(x) = - \sum_{|\lambda| < \lambda_{\text{sm}}} \left(1 - \frac{\lambda}{2} \right) \sum_c (\psi_\lambda^c(x), \gamma_5 \psi_\lambda^c(x)), \quad (4)$$

summed over color c and with λ_{sm} as an UV cut-off. Our intention was to study the topological charge density at *all scales*, in particular the spectral representation in terms of overlap modes defining $q_{\lambda_{\text{sm}}}(x)$. Also, we had the opportunity to evaluate the topological charge density without filtering (i.e. at the resolution scale a) on the Linux cluster of the LRZ in Munich. We call this the scale- a topological density $q(x)$ in contrast to $q_{\lambda_{\text{sm}}}(x)$ defined with UV smoothing. (For details see Ref. [11].)

2 Topological Density with Different Resolution

Figure 1 shows the topological density calculated with four different smoothing scales λ_{sm} given in units of $1/a$. The presentation is in the form of isosurfaces at a fixed value of $|q(x)| = q_{\text{cut}}$. With increasing λ_{sm} , the number and shape of the visible clusters changes. The given configuration has $Q = 1$.

Therefore exactly one zero mode exists. In Fig. 2 we show two extreme cases, the highly localized contribution of the single zero mode alone (left) and the scale- a topological density (right). For the same value of q_{cut} the isosurfaces of the latter fill the whole volume, separating essentially a single positive from a single negative cluster. The net charge is naively expected to reside in an unpaired instanton (located at the zero mode). Actually, however, the positive and negative charge (differing by one) is globally distributed over the two clusters.

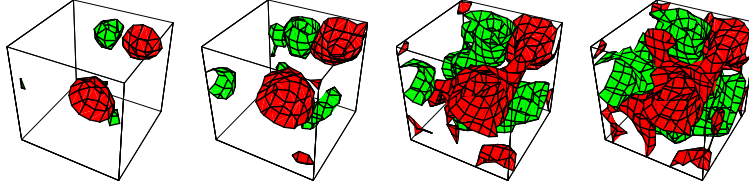


Fig. 1 Distribution of the topological charge density in a given time slice of a $12^3 \times 24$ lattice at $\beta = 8.10$: the spectral cut-off $a\lambda_{\text{sm}} = 0.14, 0.28, 0.42, 0.56$ (from left to right). The isosurfaces are shown for $q(x) = \pm 0.0005$. Colors red/green denote the sign of topological charge. Fig. from [9].

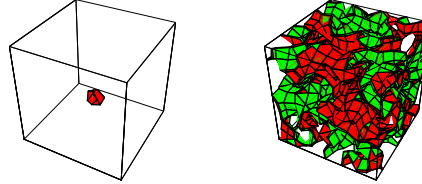


Fig. 2 The same plot as in Fig. 1 for the zero mode contribution (left) and the unfiltered density (right). Fig. from [9].

3 Cluster Analysis

More quantitative information can be obtained from a cluster analysis. The value q_{cut} , that has characterized the isosurfaces in Figs. 1 and 2, is now treated as a running parameter. The region characterized by $|q(x)| > q_{\text{cut}}$ (i.e. the interior of the isosurfaces) consists of some number of mutually disconnected clusters. We have classified them according to their size and other properties, for example their fractal dimension. Results of the cluster analysis are presented in Fig. 3. In Fig. 3a we show the number of clusters as function of $q_{\text{cut}}/q_{\text{max}}$ for three lattices characterized by different coarseness. Except for the coarsest lattice with $\beta = 8.1$ ($a = 0.142$ fm), the behavior is similar. Around $q_{\text{cut}}/q_{\text{max}} = 0.2 \dots 0.25$ the multiplicity of clusters reaches a maximum with a cluster density of $\mathcal{O}(75 \text{ fm}^{-4})$ for $\beta = 8.45$ ($a = 0.105$ fm). The density is even higher for the finer lattice with $\beta = 8.60$ ($a = 0.096$ fm). In the limit $q_{\text{cut}}/q_{\text{max}} \rightarrow 0$ the number of clusters reduces to the two oppositely charged global clusters. Figure 3b shows the volume fraction of the biggest cluster relative to all clusters. Except for the coarsest ($\beta = 8.1$) lattice, above $q_{\text{cut}}/q_{\text{max}} = 0.2$ where the number of clusters is still growing towards the maximum, this fraction is small ($< 10\%$). It changes rapidly below $q_{\text{cut}}/q_{\text{max}} = 0.2$ and approaches 50% for $q_{\text{cut}}/q_{\text{max}} < 0.1$ and remains so in the limit when only the two biggest clusters remain. The distance between the two largest clusters is shown in Fig. 3c. The “distance” is defined as the *maximum* taken over all points in one cluster of the *minimal distance* to any point of the other cluster. It approaches $2a$ for $q_{\text{cut}}/q_{\text{max}} < 0.1$, meaning that the two clusters are closely entangling each other. There are no points deep in the interior, such that the clusters must be considered to be of lower dimension than $4d$. Figure 3d shows the connectivity (explained in [11]) of the biggest

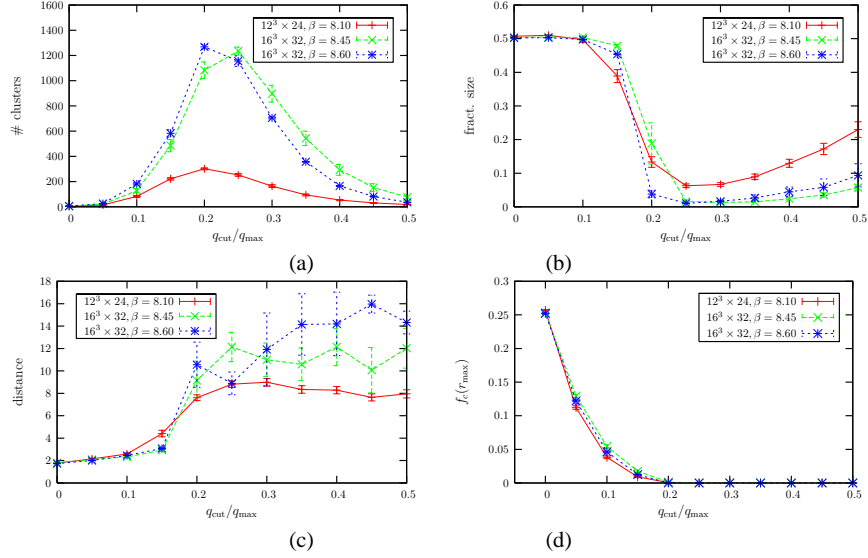


Fig. 3 Cluster analysis of the unfiltered topological density: the q_{cut} -dependence is shown (a) of the number of separate clusters, (b) of the volume of the largest cluster relative to all clusters, (c) of the distance between the two largest clusters in lattice units and (d) of the connectivity describing cluster percolation [11]. The data is plotted for the $12^3 \times 24$ lattice configurations at $\beta = 8.10$ (red), for the $16^3 \times 32$ lattice configurations at $\beta = 8.45$ (green) and for the $16^3 \times 32$ lattice configurations at $\beta = 8.60$ (blue). Fig. from [11].

cluster, describing the ability to span the whole lattice. The connectivity signals the onset of percolation which begins below $q_{\text{cut}}/q_{\text{max}} = 0.2$, too. All this confirms the description of “melting instantons” given earlier by the Kentucky group [12–14].

The meaning of the cluster analysis is geometrically visualized in Fig. 4, again contrasting the scale- a density with the filtered density. Both types of clusters are presented as a function of q_{cut} . The upper row shows, say for $q_{\text{cut}}/q_{\text{max}} \approx 0.2$, that more and more irregular, spiky clusters of the unfiltered density are popping up before percolation sets in. The lower row demonstrates that the number of clusters of the filtered density remains small and practically independent of q_{cut} . The density is $\mathcal{O}(1 \text{ fm}^{-4})$, that means comparable with what has been estimated for the instanton density. Of course, with lowering q_{cut} , the clusters slightly grow before they eventually merge. Coalescence happens finally below $q_{\text{cut}}/q_{\text{max}} = 0.1$. We see that the UV smoothed density exhibits cluster properties similar to the instanton model [19] or what cooling studies on the lattice have shown earlier [20, 21].

4 Fractal Dimensions

The visualization in three dimensions does not immediately expose the (fractal) dimension of the clusters of the scale- a topological density. We have measured the

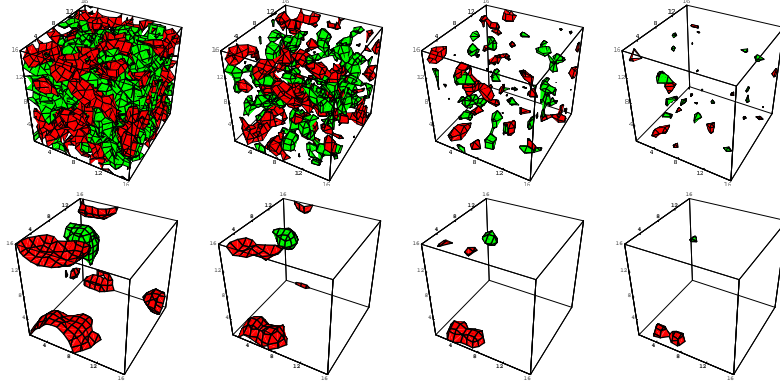


Fig. 4 Isosurfaces of topological charge density with $|q(x)|/q_{\max} = 0.1, 0.2, 0.3, 0.4$, in one timeslice of a single $16^3 \times 32$ configuration at $\beta = 8.45$. The upper pictures are based on the scale- a density, the lower pictures on the eigenmode-truncated density with $a\lambda_{\text{sm}} = 0.076$. Color encodes the sign of the charge enclosed by the isosurface. Fig. from [10].

(fractal) dimension of these clusters by a random walk method. While the cut-off q_{cut} defines the extension of the clusters as discussed above, a random walk is arranged inside the biggest cluster that is unable to penetrate the (fractal) border. A rough estimate of the dimensionality of the cluster at the respective level of q_{cut} can be inferred from the return probability to the starting point of the random walk. In d^* dimensions it behaves as a function of the number of steps like $P(\mathbf{0}, \tau) = 1/(2\pi\tau)^{d^*/2}$. Figure 5 shows the observed power like behavior for different q_{cut}/q_{\max} . The dimensions d^* extracted from this study are shown in the legend. This analysis reveals a continuous change of the fractal dimension from $d^* < 1$ (characterizing the irregular spikes) to $d^* \approx 3$ (characterizing the 3D membranes) with a lowering cut-off $q_{\text{cut}}/q_{\max} = 0.4 \dots 0.0$.

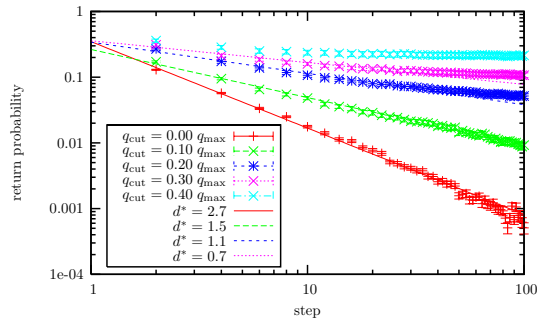


Fig. 5 The return probability of random walks in the biggest cluster of the scale- a topological density as a function of the step number, and the fractal dimensions inferred from that for various lower cut-off values q_{cut} . Fig. from [11].

5 Smearing vs. Filtering

The similarity of the filtered topological density to clusters obtained earlier by smearing methods can be studied more in detail by direct comparison. First let us recall that the overlap operator is *not ultralocal*. Even the scale- a topological density given by overlap fermions represents some inherent non-locality of the overlap operator [22]. This is seen by considering the two-point function of the topological density. Theoretically, one expects that it is negative for all non-zero distances, with an infinite, δ -like contact term at vanishing distances. The two-point function actually measured is shown as the green curve in Fig. 6a. One needs to go to larger β (a finer lattice) in order to see the positive core slowly shrinking and the minimum becoming deeper. To compare with smearing, the alternative measurement of

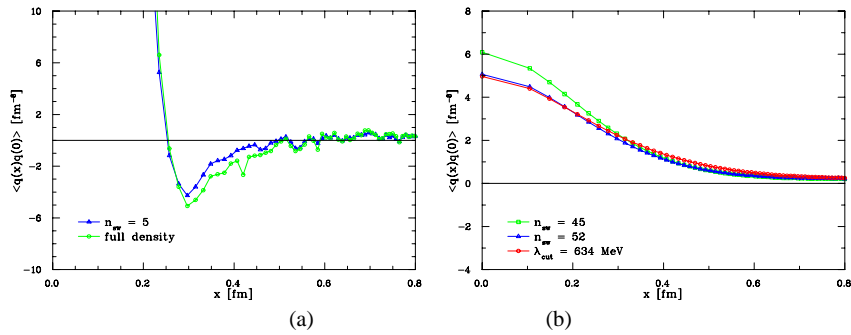


Fig. 6 Left: the two-point function of the fermionic topological density at scale a (green) compared with the bosonic definition after 5 steps of stout-link smearing (blue). Right: the two-point function of the fermionic topological density with an UV cut-off at $\lambda_{\text{sm}} = 634$ MeV (red) compared with the bosonic definition after 52 steps of stout-link smearing (blue) when the correlator is fitted best. The best point-by-point matching of the density $q_{\lambda_{\text{sm}}}$ with $\lambda_{\text{sm}} = 634$ MeV is achieved with 45 steps. For this case of less smearing the correlator is steeper. Fig. from [23].

the topological density (and of the two-point function) uses an improved bosonic definition of the topological charge density, essentially

$$q(x) = \frac{1}{16\pi^2} \text{tr}(\mathbf{E}(x) \cdot \mathbf{B}(x)), \quad (5)$$

in terms of an highly improved electric and magnetic field strength [24], that includes plaquettes and bigger loops. To apply it to a generic lattice configuration requires a few iterations of smearing (actually, of stout link smearing with respect to an overimproved action [25]) before integer-valued topological charges Q are measured with good precision. Figure 6a shows that the overlap definition and the bosonic definition of the topological density agree best to reproduce a similar two-point function at 5 smearing steps. Figure 6b shows the gluonic two-point function after 45 and 52 smearing steps compared with the overlap definition of the two-point function with $\lambda_{\text{sm}} = 634$ MeV. At this level of smearing, the negativity is already

washed out and extended clusters are visible. A point-by-point matching of the topological density and a matching of the two-point function is achieved with almost the same number of smearing iterations.

There are two parameters, q_{\max} and the size ρ_{inst} (historically the instanton radius) suitable to characterize each cluster. Now the size parameter ρ_{inst} is estimated by the curvature of $q(x)$ close to the maxima x_0 where $q(x_0) = q_{\max}$. In the form of a scatter plot in the plane spanned by these two parameters one can describe and compare the cluster composition of the gauge field. In Fig. 7 this is shown after 5 and 40 stout-link smearing steps. After 40 smearing steps the cluster multiplicity is essentially reduced, while an instanton-like relation (the curves drawn in Fig. 7)

$$q_{\max} = \frac{6}{\pi^2 \rho_{\text{inst}}^4}, \quad (6)$$

is enforced within some tolerance. At the same time the clusters are far from being ideal O(4) symmetric instanton solutions. The bosonic and the fermionic view of

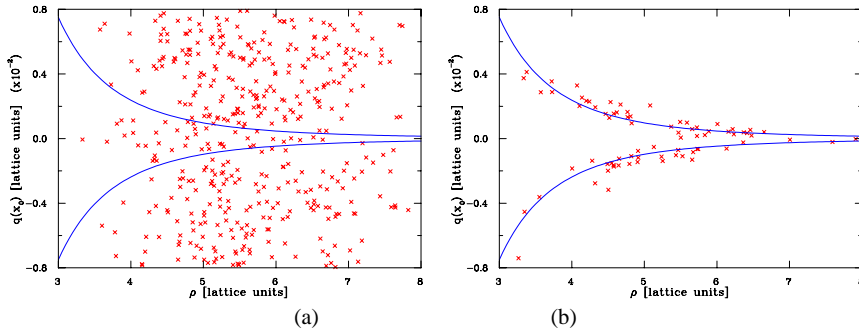


Fig. 7 The cluster content after 5 and 40 smearing steps in the q_{\max} - ρ_{inst} plane. Fig. from [23].

the cluster structure is shown in the left and right panel of Fig. 8. They show a remarkable similarity.

6 Selfduality

This leads to the question to what extent the UV smoothed *fieldstrength tensor* is *locally* selfdual or antiselfdual, or even a semiclassical (instanton) solution. Gattringer was the first to ask this question in Ref. [26]. We have applied his technique using the eigenmodes of the overlap Dirac operator. Truncating the sum over eigenvalues, an UV filtered form of the field strength $F_{\mu\nu}$ can be obtained that allows to evaluate the respective infrared (IR), UV smoothed topological charge density,

$$q_{\text{IR}}(x) \propto \text{Tr} (F_{\mu\nu}(x) \tilde{F}_{\mu\nu}(x)), \quad (7)$$

and action density

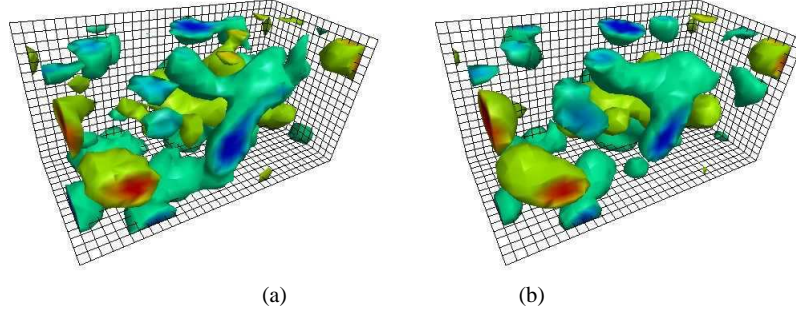


Fig. 8 The fermionic topological charge density of a $Q = 0$ configuration with $\lambda_{\text{sm}} = 634$ MeV (left) compared with the bosonic one after 48 sweeps of stout-link smearing (right). Negative: blue/green, positive: red/yellow. Fig. from [23].

$$s_{IR}(x) \propto \text{Tr} (F_{\mu\nu}(x) F_{\mu\nu}(x)) . \quad (8)$$

Analogously to the local chirality of the non-zero modes one can define the ratio

$$r(x) = \frac{s_{IR}(x) - q_{IR}(x)}{s_{IR}(x) + q_{IR}(x)} , \quad (9)$$

which can be converted to

$$R(x) = \frac{4}{\pi} \arctan \left(\sqrt{r(x)} \right) - 1 \in [-1, +1] . \quad (10)$$

Regions with $R(x) \approx -1$ or $R(x) \approx +1$ are characterized by the field strength being locally selfdual (anti)selfdual). Figure 9 shows histograms with respect to R for the whole lattice and for subsets of lattice points selected by ranking according to the action density. With higher action density (say, for $< 30\%$ of the lattice points

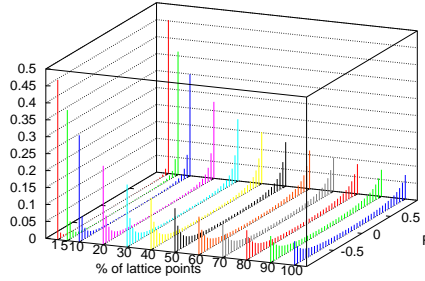


Fig. 9 Normalized histogram with respect to the UV smoothed (anti)selfduality R for different subsamples of lattice points (1%, 5%, 10% etc.) ordered with respect to the UV smoothed action. 20 overlap modes have been included in the smoothing. Fig. from [11].

forming “hot spots” of filtered action S_{IR}) the parameter R is distributed close to ± 1 (i.e. $|R| > 0.7$). Clusters with respect to $|R| > 0.98$ are overlapping with clusters of a suitably filtered topological density.

7 Localization and Local Chirality of Overlap Eigenmodes

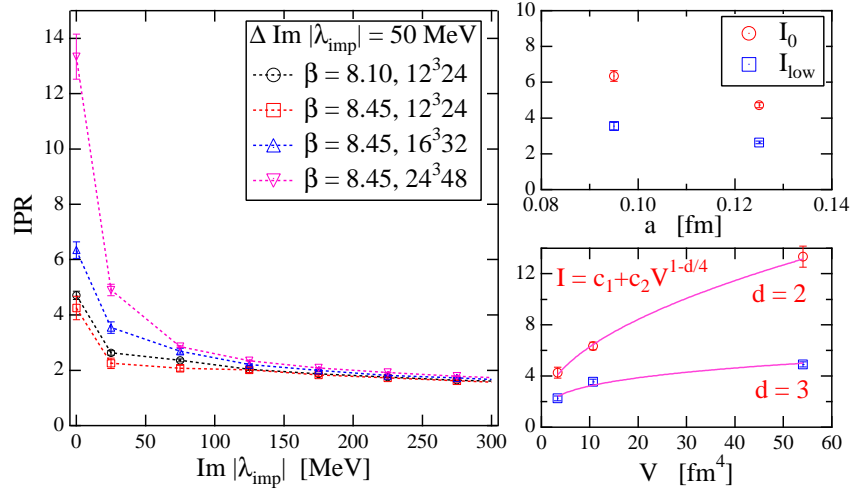


Fig. 10 IPR: the dependence on λ (left), the a -dependence (right upper), and the V -dependence (right lower). Fig. from [9].

We have also analyzed the localization behavior of individual overlap eigenmodes. The interest in the localization properties of Dirac and scalar eigenmodes has been discussed by de Forcrand [27]. In the left panel of Fig. 10 we show the average inverse participation ratio (IPR) typical for zero modes and for bins of eigenvalues in dependence on coarseness and lattice size. The localization grows approaching the continuum limit and with increasing physical volume. The right panel shows, separately for zero modes and the first bin ($|\lambda| < 50$ MeV), the change of the IPR with a and with V . From fits we have concluded that zero modes are typically 2-dimensionally extended, while the lowest non-zero modes are 3-dimensional objects.

Similar to (9) the local chirality $X(x)$ of the non-zero modes can be defined. This quantity is highly correlated with the UV smoothed topological density. For $\lambda_{\text{sm}} = 200$ MeV the correlation function between $X(x)$ and $q_{\lambda_{\text{sm}}}(y)$ is shown in Fig. 11. The correlator is positive for the lowest 120 eigenmodes within a range of distance $R < \mathcal{O}(1 \text{ fm})$.

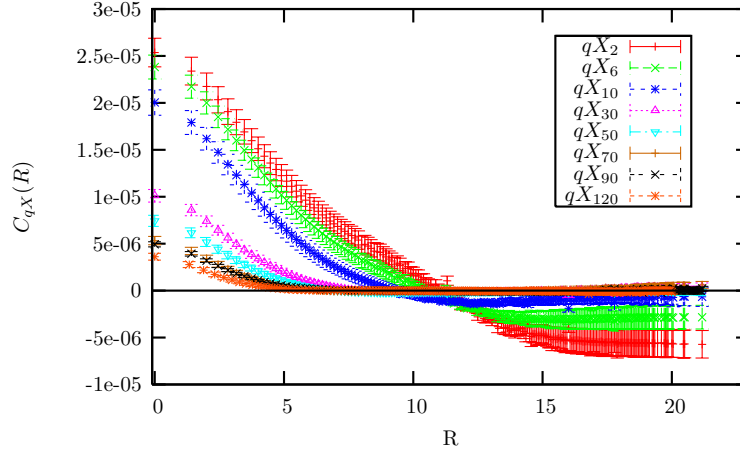


Fig. 11 The correlation function between the local chirality $X(x)$ of selected eigenmodes and the filtered topological density $q_\lambda(y)$ in a configuration with topological charge $Q = 0$. Fig. from [11].

8 Technical Details

To compute the low lying eigenvalues of the overlap Dirac operator (2) we use an adaption of the implicitly restarted Arnoldi method which is used in the ARPACK [28] library. The advantage of this method is that the action of a matrix on a vector can be computed freely without the need to express the input matrix explicitly.

The main computational challenge using the overlap Dirac operator as an input matrix is the computation of the sign function $\text{sgn}(D_W)$ in (2). We project out the lowest $\mathcal{O}(50)$ eigenvalues of D_W and treat them exactly. The rest acting in the orthogonal subspace is approximated using minmax polynomials [29]. The application of the Wilson-Dirac operator D_W on a vector, the main computational kernel of almost every lattice QCD code, is implemented in assembler and highly optimized using SSE2 instructions. The data is aligned on full cache lines and stored in a special way to make optimal use of the 128-bit XMM registers. Prefetch instructions are issued to move the data to the cache accurately timed. The SSE2 version reaches approx. 1/3 of peak performance on a $16^3 \times 32$ lattice on the Linux cluster of the LRZ.

The computation of the scale- a topological density $q(x)$ requires to evaluate the local trace over Dirac and color indices of the overlap Dirac operator with the γ_5 matrix included according to (3). This can be trivially parallelized, but is numerically extremely expensive, since the overlap operator has to be applied on $12 V_{\text{lat}}$ unit vectors. To compute $q(x)$ on one single configuration on a $16^3 \times 32$ lattice approx. $1.3 \cdot 10^4$ CPU hours for totally 1.6 million applications of the overlap Dirac operator were required.

9 Conclusions

We have confirmed that the scale- a topological density is highly singular and the topological charge of either sign is globally filling the two extended $3d$ percolating structures. A similar low-dimensionality is found for chiral zero-modes (two-dimensional) and the lowest non-chiral non-zero modes (three-dimensional). The microscopic topological density is correlated with vortices and monopoles [30].

The UV filtered topological density shows cluster properties reminiscent of instantons. We found a highly correlated behavior of a huge number of lowest modes resembling the presence of a semiclassical background. The suitably UV smoothed field strength tensor becomes selfdual (antiselfdual) at “hot spots” where the corresponding action becomes maximal. The reason for this self-organization between the fermionic modes is still unclear.

References

1. Neuberger, H.: Exactly massless quarks on the lattice. *Phys. Lett.* **B417**, 141–144 (1998). DOI 10.1016/S0370-2693(97)01368-3
2. Neuberger, H.: More about exactly massless quarks on the lattice. *Phys. Lett.* **B427**, 353–355 (1998). DOI 10.1016/S0370-2693(98)00355-4
3. Lüscher, M.: Exact chiral symmetry on the lattice and the Ginsparg-Wilson relation. *Phys. Lett.* **B428**, 342–345 (1998). DOI 10.1016/S0370-2693(98)00423-7
4. Hasenfratz, P., Laliena, V., Niedermayer, F.: The index theorem in QCD with a finite cut-off. *Phys. Lett.* **B427**, 125–131 (1998). DOI 10.1016/S0370-2693(98)00315-3
5. Niedermayer, F.: Exact chiral symmetry, topological charge and related topics. *Nucl. Phys. Proc. Suppl.* **73**, 105–119 (1999). DOI 10.1016/S0920-5632(99)85011-7
6. Galletly, D., et al.: Quark spectra and light hadron phenomenology from overlap fermions with improved gauge field action. *Nucl. Phys. Proc. Suppl.* **129**, 453–455 (2004). DOI 10.1016/S0920-5632(03)02611-2
7. Galletly, D., et al.: Hadron spectrum, quark masses and decay constants from light overlap fermions on large lattices. *Phys. Rev.* **D75**, 073,015 (2007). DOI 10.1103/PhysRevD.75.073015
8. Göckeler, M., et al.: Simulating at realistic quark masses: light quark masses. *PoS LAT2006*, 160 (2006)
9. Koma, Y., et al.: Localization properties of the topological charge density and the low lying eigenmodes of overlap fermions. *PoS LAT2005*, 300 (2006)
10. Ilgenfritz, E.M., et al.: Probing the topological structure of the QCD vacuum with overlap fermions. *Nucl. Phys. Proc. Suppl.* **153**, 328–335 (2006). DOI 10.1016/j.nuclphysbps.2006.01.028
11. Ilgenfritz, E.M., et al.: Exploring the structure of the quenched QCD vacuum with overlap fermions. *Phys. Rev.* **D76**, 034,506 (2007). DOI 10.1103/PhysRevD.76.034506
12. Horváth, I., et al.: On the local structure of topological charge fluctuations in QCD. *Phys. Rev.* **D67**, 011,501 (2003). DOI 10.1103/PhysRevD.67.011501
13. Horváth, I., et al.: Low-dimensional long-range topological charge structure in the QCD vacuum. *Phys. Rev.* **D68**, 114,505 (2003). DOI 10.1103/PhysRevD.68.114505
14. Horváth, I., et al.: Inherently global nature of topological charge fluctuations in QCD. *Phys. Lett.* **B612**, 21–28 (2005). DOI 10.1016/j.physletb.2005.03.004
15. Thacker, H.B.: D-branes, Wilson bags, and coherent topological charge structure in QCD. *PoS LAT2006*, 025 (2006)

16. Thacker, H.B.: Topological charge and the laminar structure of the QCD vacuum. *AIP Conf. Proc.* **892**, 223–226 (2007). DOI 10.1063/1.2714378
17. Thacker, H.B.: Melting instantons, domain walls, and large N . *PoS LAT2008*, 260 (2008)
18. Ginsparg, P.H., Wilson, K.G.: A remnant of chiral symmetry on the lattice. *Phys. Rev.* **D25**, 2649 (1982). DOI 10.1103/PhysRevD.25.2649
19. Schäfer, T., Shuryak, E.V.: Instantons in QCD. *Rev. Mod. Phys.* **70**, 323–426 (1998). DOI 10.1103/RevModPhys.70.323
20. Negele, J.W.: Instantons, the QCD vacuum, and hadronic physics. *Nucl. Phys. Proc. Suppl.* **73**, 92–104 (1999). DOI 10.1016/S0920-5632(99)85010-5
21. García Pérez, M.: QCD vacuum structure. *Nucl. Phys. Proc. Suppl.* **94**, 27–34 (2001). DOI 10.1016/S0920-5632(01)00924-0
22. Horváth, I., et al.: The negativity of the overlap-based topological charge density correlator in pure-gluon QCD and the non-integrable nature of its contact part. *Phys. Lett.* **B617**, 49–59 (2005). DOI 10.1016/j.physletb.2005.04.076
23. Ilgenfritz, E.M., et al.: Vacuum structure revealed by over-improved stout-link smearing compared with the overlap analysis for quenched QCD. *Phys. Rev.* **D77**, 074,502 (2008). DOI 10.1103/PhysRevD.77.074502
24. Bilson-Thompson, S.O., Leinweber, D.B., Williams, A.G.: Highly-improved lattice field-strength tensor. *Ann. Phys.* **304**, 1–21 (2003). DOI 10.1016/S0003-4916(03)00009-5
25. Moran, P.J., Leinweber, D.B.: Over-improved stout-link smearing. *Phys. Rev.* **D77**, 094,501 (2008). DOI 10.1103/PhysRevD.77.094501
26. Gatttringer, C.: Testing the self-duality of topological lumps in $SU(3)$ lattice gauge theory. *Phys. Rev. Lett.* **88**, 221,601 (2002). DOI 10.1103/PhysRevLett.88.221601
27. de Forcrand, P.: Localization properties of fermions and bosons. *AIP Conf. Proc.* **892**, 29–35 (2007). DOI 10.1063/1.2714343
28. <http://www.caam.rice.edu/software/ARPACK/>
29. Giusti, L., Hoelbling, C., Lüscher, M., Wittig, H.: Numerical techniques for lattice QCD in the epsilon-regime. *Comput. Phys. Commun.* **153**, 31–51 (2003). DOI 10.1016/S0010-4655(02)00874-3
30. Ilgenfritz, E.M., et al.: Localization of overlap modes and topological charge, vortices and monopoles in $SU(3)$ LGT. *PoS LAT2007*, 311 (2007)